Paste 2023 – GW Wilson, NA Beier, DC Sego, AB Fourie & D Reid (eds)

doi:10.36487/ACG_repo/2355_14

Arctic backfilling: challenges and lessons-learned

L-P Gélinas *Agnico Eagle Mines Ltd., Canada*

J Alcott *Agnico Eagle Mines Ltd., Canada*

Abstract

Backfill is an inherent component of the mining at Agnico Eagle Mines' (AEM) arctic operations in Canada, Nunavut, including Amaruq, Meliadine and Hope Bay. Backfill quality is essential to limit the dilution during the mining of secondary stopes and to optimise the mining sequence in this cost-challenging environment. Backfilling with cemented rockfill (CRF) or cemented paste backfill (CPB) in Canadian Arctic conditions is demanding since many assumptions and experiences acquired in warmer temperatures are no longer applicable. Through innovative laboratory techniques, in-situ monitoring and operational lessons learned, AEM operates with various backfilling techniques adapted to the Arctic environment.

Keywords: *Cemented Rockfill, cemented paste tailings, arctic, permafrost, compressive strength, in-situ monitoring*

1 Introduction

The use of backfill is common in underground mines. Over the years, operators have developed a wide range of initiatives to reduce costs and increase operational effectiveness. These techniques include calculating required backfill strength, mixing techniques, and QA-QC programs. These have been adapted through trial and error, meaning that many mining engineering decisions for backfill are based on rules of thumb (Hughes 2014; de la Vergne 2000). For Agnico Eagle Mines (AEM), adapting these backfilling experiences to new Arctic underground operations brought new challenges. The initial strategy was to reproduce the techniques developed for more-southernly mines (mainly in the Abitibi region) – including recipe, strength calculation, cement type and mixing techniques - and apply these to northern projects. Through a rigorous risk management process at the project level, these assumptions were challenged and had to be revised to consider the Canadian Arctic context. Many southern backfilling practices, such as cement type and hydration time, did not apply to the North. This paper summarises the laboratory approach, the in-situ monitoring data and results obtained, and the operational lessons learned from three different AEM arctic operations: Meliadine, Amaruq, and Hope Bay.

2 Mine general descriptions

2.1 Meliadine

As seen in Figure 1, the Meliadine (MLD) mining complex is in the Kivalliq region of Nunavut near the western shore of Hudson Bay in Northern Canada. The property is in low-lying topography with numerous lakes, about 60 m above sea level. Surface waters are usually frozen from early October until early June. Mining equipment, fuel and dry goods are transported on the annual warm-weather sealift by barge to Rankin Inlet via Hudson Bay and then using a 33 km all-weather road to the mine site.

This operation uses cemented paste backfill and cemented rockfill to backfill long-hole transverse (75%) and longitudinal stopes (25%). Stopes are approximately 25 m in height (back-to-back) and 18 m wide, with an

average thickness of 8 m for transverse and 5.5 m for longitudinal mining. On 31 December 2021, MLD was estimated to host 3.7 million ounces of gold in proven and probable mineral reserves (19.2 million tonnes grading 5.93 g/t gold), mostly underground at depth. The backfilling target is 1,800 tonnes of cemented paste and rockfill per day combined (AEM 2022).

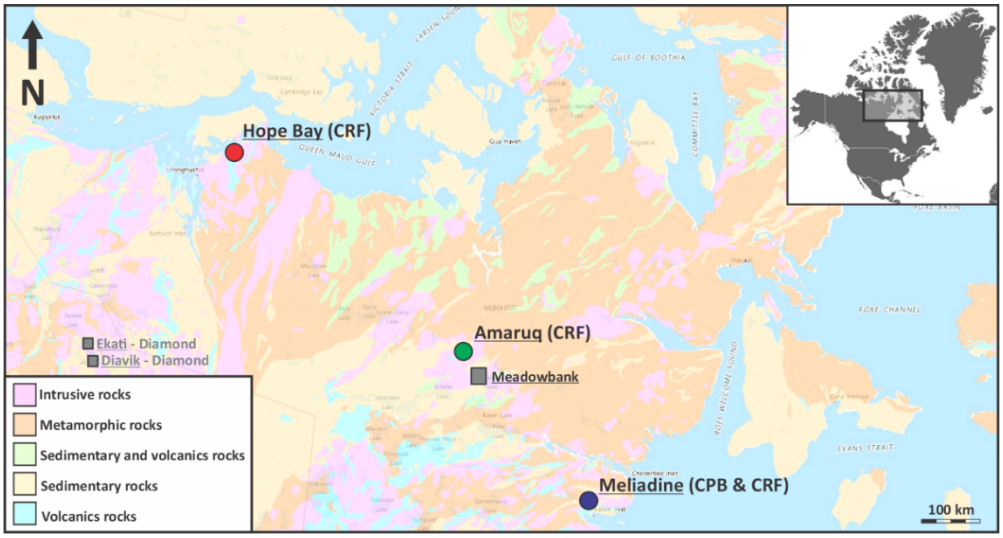

Figure 1 Agnico Eagle Mines advanced project and mines in Nunavut, Canada

2.2 Amaruq

The Amaruq (AMQ) underground mine is part of the Meadowbank (MBK) mining complex, located in the Kivalliq region of Nunavut, 400 km northwest of the Hudson Bay shore in Northern Canada, as seen on the map of Figure 1. In February 2021, the construction of the AMQ underground project started, and the first gold was poured in late 2021; commercial production began in the second half of 2022. The objective is to mine the higher-grade underground portions of the deposit simultaneously with open pit production. AEM released the AMQ Underground Project PFS in February 2020 with an assumed production plan of 3.303 million tonnes of ore grading at 5.43 g/t (AEM 2022). Ore from the AMQ open pit and underground mines is hauled by long-haul trucks and treated at the nearby Meadowbank processing plant. The current plans for this underground mine are to mine only within the permafrost and will not be heated.

Mining equipment, fuel and dry goods are transported on the annual warm-weather sealift by barge via Baker Lake, then using a 110 km all-weather road from the Inuit village of Baker Lake to Meadowbank and another 73 km to AMQ. Given the distance between the mill and the mine, cemented paste backfill could not be used. The production plan relies on the placement of 1000 tonnes per day of cemented rockfill. Stopes are approximately 25 m in height (back-to-back), between 10 to 20 m wide, with an average thickness of 10 m, depending on lithology and mining method (i.e., transverse or longitudinal).

2.3 Hope Bay

The Hope Bay (HOP) property is in the Kitikmeot region of Nunavut, approximately 685 km northeast of Yellowknife and 125 km southwest of Cambridge Bay. The Doris underground mining sector produced gold from early 2017 until Agnico Eagle Mines acquired TMAC Resources Inc in 2021. Mining operations were temporarily halted in September 2021. On 31 December 2021, it was estimated that HOP (Doris, Madrid, and Boston deposits) contained probable mineral reserves of 3.33 million ounces with 16.0 million tonnes at 6.50 g/t gold (AEM 2022). Stope size varies depending on the mining zones and method (i.e., longitudinal or transverse), but in general, stopes are 20 m high, 5 m wide and a maximum of 25 m along strike.

Mining equipment, fuel and dry goods are transported on the annual warm-weather sealift by barge to Roberts Bay and then by a short 10 km all-weather road to the HOP processing plant. Backfill is currently planned to be cemented rockfill and dry rockfill.

3 Canadian Arctic-specific hydrogeological contexts

These three underground mines are primarily developed and operated under conditions of permanently frozen rock with a rock mass temperature below 0°C. Both AMQ and HOP are currently planned to be mined within the permafrost. As mining extends below the permafrost at MLD, this creates the additional challenge of managing deep groundwater inflow into the underground excavations. MLD mine ventilation also differs from the AMQ and HOP. At MLD, the air is heated to keep the temperature UG above freezing, which is not the case for AMQ and HOP. Understanding hydrogeological context, water chemistry, and curing temperature is essential for backfill recipe design. In an Arctic context, one can gain backfill early and ultimate strength for a given recipe by increasing the initial temperature of the water, cement, and waste. Heating water for slurry or paste mixing can sometimes come at a lower cost than increasing binder content.

The salinity of underground water at these mines is controlled by two main factors: the addition of brine, which is essentially $CaCl_2$ mixed with water, and the naturally occurring mineral salts dissolved in groundwater. Mixing water salinity is a risk identified, requiring early evaluation at the project stage. Using the geochemical modelling for the water balance study, it was possible to reproduce the projected water salinity in the lab and evaluate its impact on the hydration reaction for cemented paste and rock backfills. If operations mainly control salinity, the primary ions controlling the water salinity will differ from those found in groundwater. The effect of chloride (salt) concentration will vary for NaCl versus $CaCl_2$. The salt content of the interstitial tailings and mixing waters also influence mechanical strength development. The Unité de Recherche et de Service en Technologie Minérale (URSTM) lab testing (2012) shows a complex relationship between temperature, chloride concentration, and early-age mechanical strength. Under certain conditions, chloride concentrations can lead to either a decrease or increase in mechanical strength. The groundwater chemistry for the three mine sites is summarised in Table 1. The groundwater regime at MEL has a seawater signature. The primary chloride ions are from NaCl, which means a higher sodium concentration. At AMQ, where groundwater infiltration is less significant, the salinity will come largely from $CaCl_2$ introduced by the operation, resulting in a higher calcium concentration. The HOP deep groundwater is connate, which means very old. This connate water is highly saline and can have elevated concentrations of major ions and metals. The calcium, chloride and sodium concentrations are high and generally increase with depth (SRK 2017).

Table 1 Simplified water chemistry of HOP (Madrid North 548m), MEL (water stope) and AMQ (ST-W-20)

Parameters	Units	HOP	MLD	AMQ
Alkalinity	*mg/L*	2.0	37.0	38.0
Calcium	*mg/L*	4 960.0	38.0	254.0
Magnesium	*mg/L*	69.5	34.9	12.7
Potassium	*mg/L*	39.0	14.9	17.5
Sodium	*mg/L*	7 290.0	209.0	8.3
Chloride	*mg/L*	1 900.0	570.0	490.0
Sulphate	*mg/L*	981.0	110.0	14.0
Salinity	*%*	3.2	1.0	0.9

4 Water/cement interaction: Example of AMQ and HOP CRF

Cemented rock fill (CRF) is a waste rock and cement slurry mixture. As mentioned, the higher salinity of the mixing water used for the cement slurry at AEM's arctic operations complicates CRF design. Therefore, flow tests were conducted to validate that there was no negative interaction between mine water and cement (HE and GU). Flow tests were initially developed for mortar slurry (ASTM 2011). They use a high-velocity mixer to mix different types of water and cement. Temperature and flow are measured at different intervals as the cement hardening process accelerates. The instruments used are illustrated in Figure 2. For this experiment, 600 ml of slurry was prepared. The mixer operated at 4,000 rpm for 15 seconds, during which all the cement solids were added to the mix water, followed by 35 seconds at 12,000 rpm. The flow tests were done at 10, 30, and 60 minutes with a cone and board. Over time, the procedure and the mixing water temperature were adjusted to better represent site conditions.

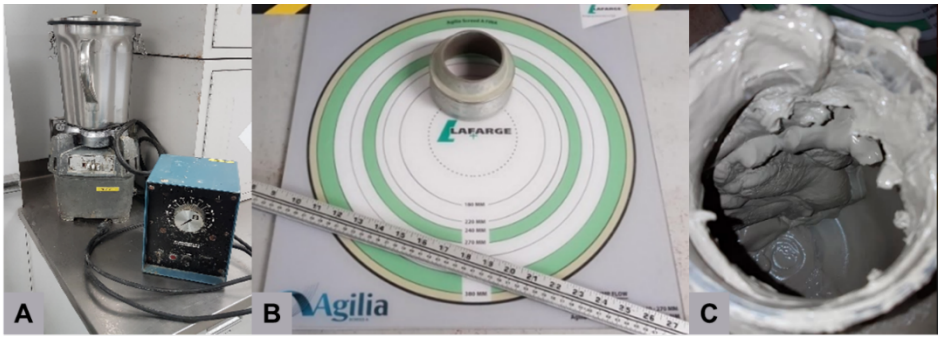

Figure 2 (a) Waring blender, (b) cone and board used to measure the flow (ASTM 2011) and (c) the inside of the blender when a recipe has set (Lafarge 2020)

Table 2 presents some flow test results for AMQ and HOP. These tests aimed to determine whether AMQ and HOP mine waters would interact negatively with High Early (HE) type cement. To better understand potential impacts, the considered water chemistry end-members were municipal tap water and a mix of tap water with 10% $CaCl_2$ which is theoretically the highest salinity that could be encountered underground. For both AMQ and HOP, the salinity of each site's process water lies between these two extremes. No flow was observed for slurries containing 10% $CaCl_2$ and HE. The initial temperature of the mixture in the blender immediately after the mixing is essential for controlling flowability. With time the procedure was refined. At first, the mixing was done with water at a lab temperature of 21°C for the AMQ samples. At 21°C, the hydration reaction occurs so rapidly that for a mixture composed of municipal water, the slurry temperature rises from 21 to 34.5°C in seconds. These temperature conditions are unlikely to be found in an Arctic operation, and a retardant would likely be added to increase flowability in a southern operation. For the HOP testing, the initial temperature of the water before mixing with cement was set to 10°C. The initial water temperature variation explains the difference between the AMQ and HOP results for similar mixes. For HOP, the HE slurry prepared with 10% $CaCl_2$ showed a significant increase in temperature from 10°C to over 20°C. No flow was observed even if the temperature was lower than the AMQ samples.

Table 2 Flow results with three types of water for AMQ and HOP

Mine	Cement Type	Water type	Initial temperature (°C)	Initial flow (mm)	Flow at 10 min (mm)	Flow at 30 min (mm)	Flow at 60 min (mm)
AMQ	Type 30/ HE	Municipal Water (Montréal)	34.5	190	188	183	174
AMQ	Type 30/ HE	Mine process water	40	148	117	No Flow	No Flow
AMQ	Type 30/ HE	Lab. Water @ 10% $CaCl_2$	44.6	No Flow	No Flow	No Flow	No Flow
HOP	Type 30/ HE	Municipal Water (Seattle)	10	121	124	110	88
HOP	Type 30/ HE	Mine process water	9.7	130	110	108	98
HOP	Type 30/ HE	Lab. Water @ 10% $CaCl_2$	21	No Flow	No Flow	No Flow	No Flow

Although using higher salinity mixing water can be advantageous for protecting the CRF mix from freezing, increased salinity can also accelerate the hydration reaction. A critical salinity level ensures the slurry will not stick to the scoop bucket and will allow optimal CRF preparation and placement. Higher salinity can also generate small, coagulated cement particles that will limit bond creation between the waste rock material.

Water salinity values may vary over mine life, so a procedure must be in place to identify variations that could impact backfill reliability. Flow tests are essential, fast, cheap, and easy to validate potential issues between cement types and water chemistry. A testing program should consider various UG water sources and initial temperatures. Even more straightforward tests can be done on-site where a slurry sample is kept in a recipient, cured at the same temperature as UG and the setting time is measured. Another consideration during these tests is how the slurry is brought to the stope and mixed. For example, a surface slurry plant with ready-mix trucks or an underground distribution system will require a slurry with a longer setting time than a system where the slurry is prepared with a mobile slurry mixer at the stope. These options will impact slurry design and require a complete trade-off study to validate the suitability of CRF for an Arctic project.

5 Temperature and cement type: The example of MEL CPB

Most AEM mines use slag-based cement for the preparation of cemented paste backfill. This blended cement type is not sensitive to sulphate attack. Slag mixed with 10-30% General Use (GU) cement is the optimal blend. The GU cement generates sufficient early-age resistance (less than three days) by providing alkali activation, and the slag helps the backfill to achieve higher final strength. During the initial lab testing program for MLD (URSTM 2012 and Kalongi 2016), high UCS results were obtained for 2.5% blended slag-GU:80-20% binder cured at 23°C (i.e., UCS> 500 kPa after 28 days). However, the northern permafrost conditions meant these results, particularly the curing environment, could not be achieved. Mechanical strength development is highly affected for samples cured at low temperatures. For the MEL CPB, strengths below 300 kPa were obtained for a recipe prepared with 7% slag-GU after 28 days of curing time at 2°C. Concerns regarding relatively low strength at lower curing temperatures led to the investigation of HE cement as an alternative to slag-GU-based cement at MEL. In 2014, testing by URSTM showed that the 3, 4, and 5% slag-HE:80-20% produced similar results to slag-GU binder, allowing the development of good mechanical strengths under higher temperatures (i.e., UCS higher than 700 kPa after 56 days of curing at 21°C). However, the hydration reaction of the slag-HE binder was slower and suffered from the same issues as the slag-GU binder at low curing temperatures (2°C), which meant that at 28 days, the UCS values were below 200 kPa. Based on these results, a decision was made to consider a 100% HE binder for its strength properties at lower curing temperatures.

In 2015, it was difficult to obtain representative tailings since MEL was not yet in operation, limiting the number of samples that could be prepared. Major assumptions were made regarding the mine water

geochemistry and, more importantly, the curing temperature of the cemented paste backfill (URSTM, 2015). Beya (2016) studied temperature evolution at MLD in the paste line and a stope poured within permafrost. The initial assumptions were that paste exiting the plant would be 10°C and that a temperature increase would occur during transport. The COMSOL model predicted that the temperature would rise to 14°C in the pipe and that the temperature of the paste at the stope walls would be at 3°C after 28 days. These predictions were validated with a scale-model in the lab, but there were no in-situ measurements to confirm the temperature hypotheses.

To validate these temperature assumptions, an in-situ thermal instrumentation campaign was undertaken. Thermocouples were placed in open stopes, which were subsequently backfilled. Next, the thermocouple cables were attached to a grouting tube and placed in a stope. Two type T-thermocouple cables (1 & 2) were placed in the middle of the plug pour, and two thermocouples (3 & 4) were in the mass. These cables were connected to a four-channel Hobo logger. Figure 3 shows the tools and setup used for these installations. The main goal of the instrumentation campaign was to keep the budget down so that this setup could be easily and reliably reproduced.

Figure 3 Pictures showing in (a) the materials used for stope instrumentation: T-type cables, Hobo logger and infrared thermometer. Cable with the thermocouples attached at the undercut for the stope 200-150-1100 (b), view of the overcut of the stope 225-159-1100 (c).

Figure 4 shows the geometry of an instrumented stope. For the 225-159-1100 stope, a recipe of 5% HE binder with a 7-inch slump was used for a first pour of 2540 tonnes and a second pour of 7572 tonnes.

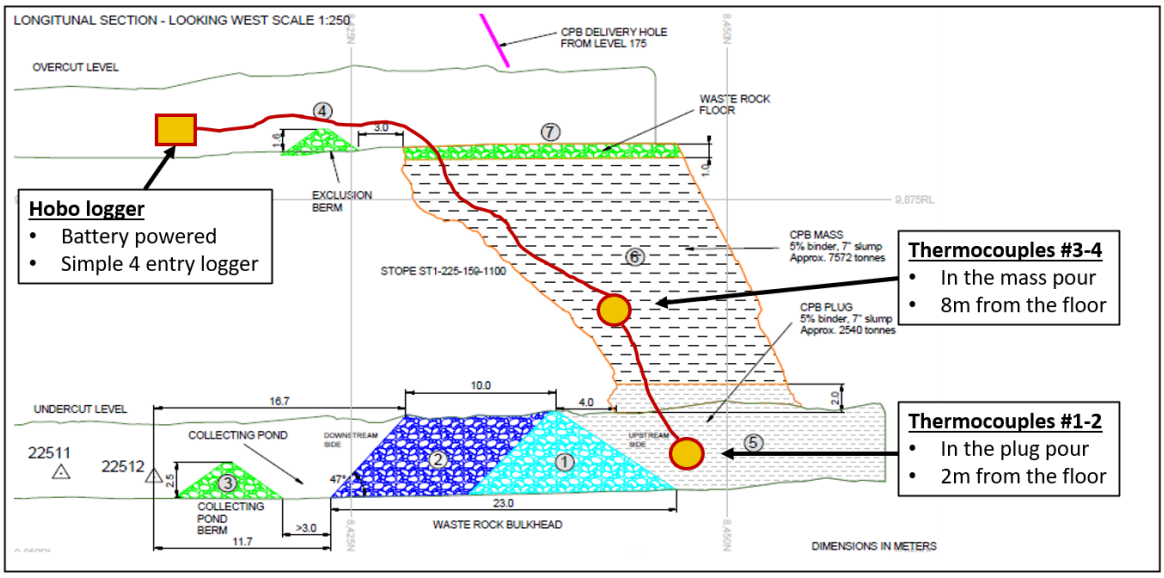

Figure 4 225-159-1100 stope geometry and the simplified thermocouples and Hobo logger setup.

Figure 5 combines thermocouple data for several instrumented stopes. Data are shown using a standard sampling rate of 1 point every 20 minutes recorded over 125 hours to compare the different installations. Data were also simplified so that temperature recording starts approximately when the paste contacts the thermocouple. For all stopes back-up, the thermocouples were installed in case of problems. As seen in Figure 5, the stope air temperature was 5°C, and the paste temperature varied between 8.5°C and 10°C before stabilising at 6.5°C for stope 200-150-1100. It is important to note that there were multiple flushes at the beginning of the pour, which explains the temperature variation before the pour stabilised. Once the hydration started, the paste temperature rose approximately 2.5°C from 6.5°C to 9°C. A few days later, when the paste reached the thermocouples 10 m above the floor of the same stope during the mass pour, the air temperature was just below 7°C. The higher air temperature is attributed to the heat the paste generated in the plug below. A flush prior to resuming the pour explains the drop in the paste temperature to 9°C before the paste reached the stope, and then the hydration process of the mass pour increased the temperature to just above 12°C. Considering a starting paste temperature of 10°C, an increase of 2°C associated with the hydration also occurred for this curve. The temperature curves from the 225-159-1100 stope (Figure 5) follow similar trends. The stope air temperature before pouring was 2°C. The paste temperature was approximately 11°C while exiting the pipe, reached 13°C, and then stabilised at 12.5°C. For the mass, the temperature air was similar. Once the thermocouple was in contact with the paste, the temperature rose to 11°C, and the hydration process increased the temperature of the paste above 15°C, stabilising at 14°C. It is important to note that all pours had 5% HE cement, except for the beginning of the mass pour for the 225-159-110 (7% HE). The difference in percentage binder may explain the 4°C temperature increase (7%) instead of the 2°C (5%) increase for the other pours.

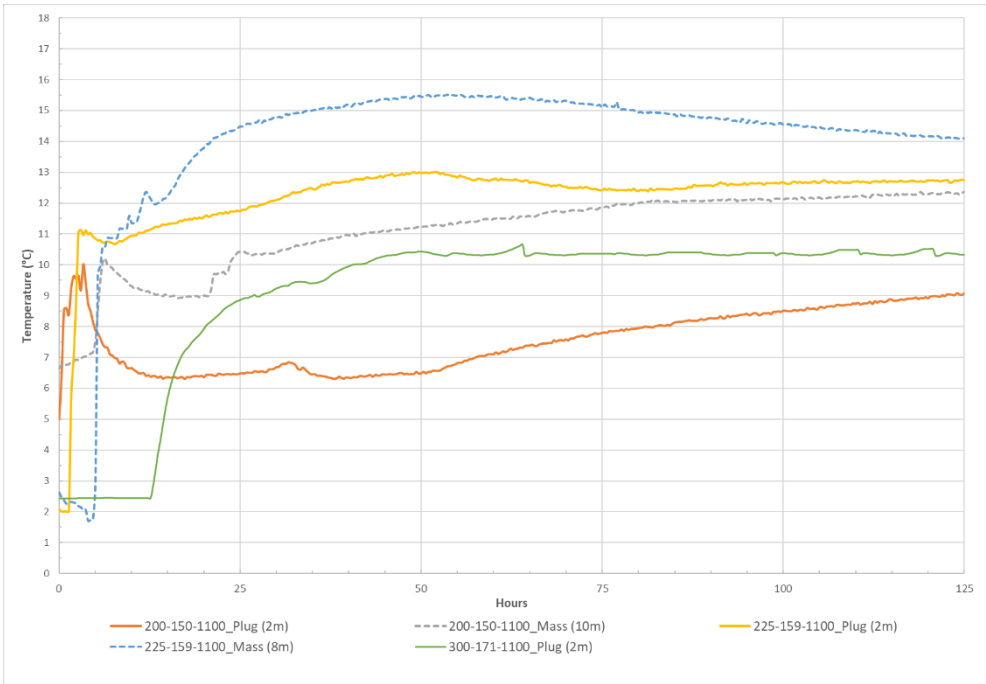

Figure 5 Combined temperature data for selected thermocouples instrumented stopes at MLD.

In Figure 6, the overcut of the 400-135-1255 stope is illustrated. Unfortunately, thermocouple instrumentation data was unavailable for measuring the paste temperature inside this stope. However, a handheld infrared thermometer was and can be routinely used to measure the rock mass surface and paste temperatures.

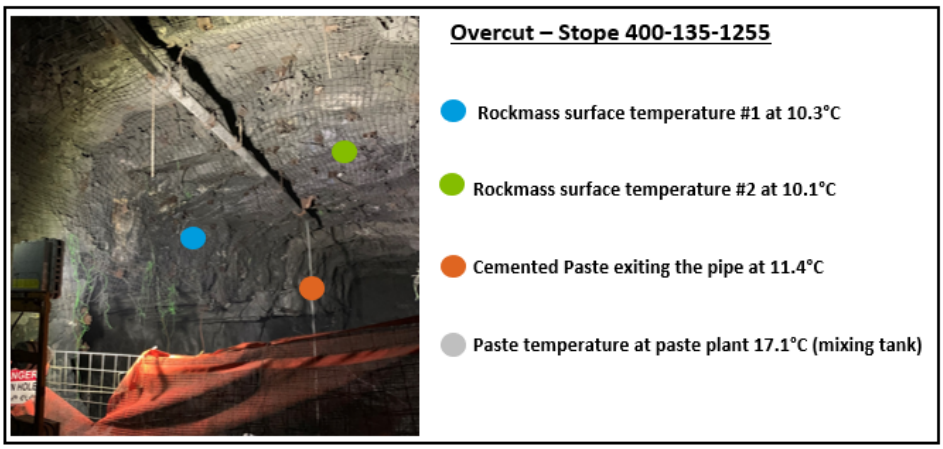

Figure 6 Overcut pictures of the stope 400-135-1255. Coloured dots show the approximate locations of the surface temperatures recorded with a handheld infrared thermometer.

Figure 7 shows UCS results with a strong relationship between UCS and temperature. Varying the curing temperature between 2, 4, 10, or 11°C for the same HE recipe and the similar water content resulted in 28-day resistance values of 264, 391, 450, and 444 kPa, respectively. The resistance data for slag-GU recipes cured at 2 and 21°C is also shown for reference. Lab and in-situ testing, from the project stage to operation, were essential for the MLD operation to deliver a high-quality paste with the required 28-day strength with optimal binder type and content.

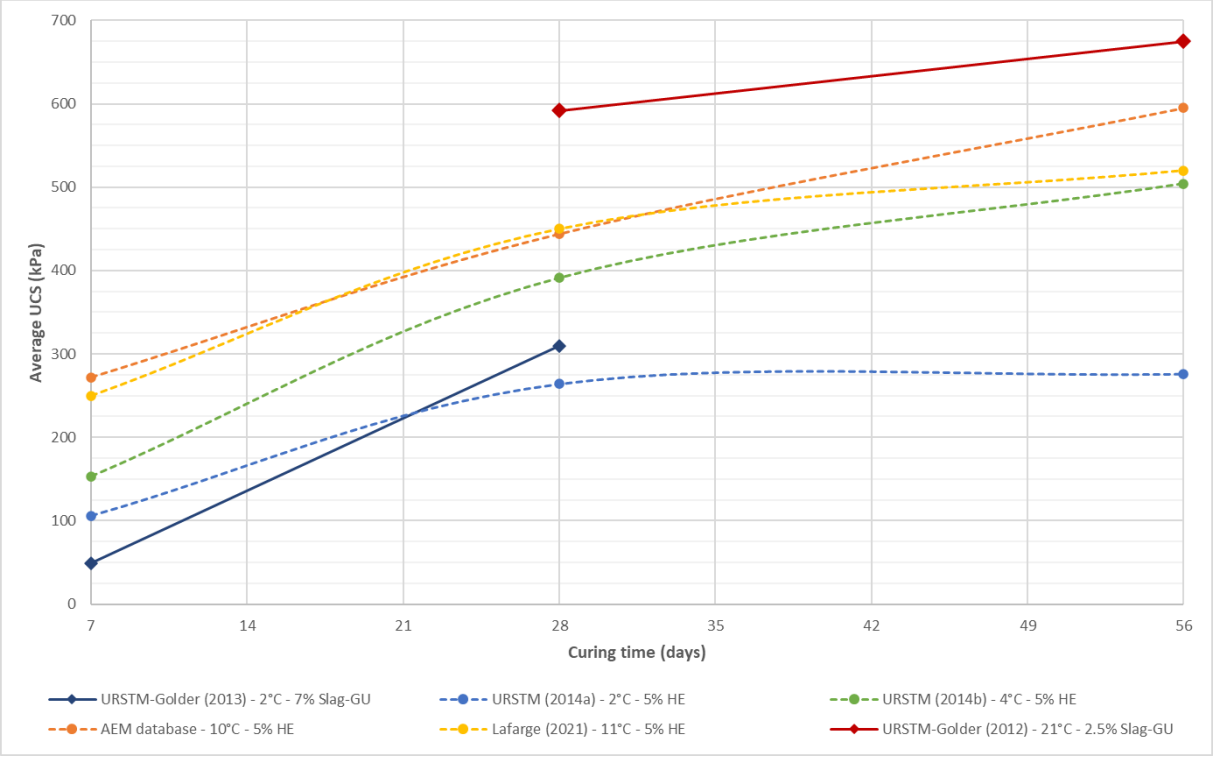

Figure 7 Compilation of UCS cemented paste backfill sample results at different curing temperatures

Initially, all tests and curing temperatures assumed a cure temperature of between 2-4°C. Based on the operational in-situ measurements, an average curing temperature of 10°C was established for the QA/QC program. For a 10°C curing temperature, the selection of HE cement instead of GU or a slag-based binder

was justified. The MLD operation continues to gain knowledge, and longer-term instrumentation is planned to validate when the temperature equilibrium occurs between rock mass and paste.

6 Particle size distribution and temperature: AMQ and HOP CRF

CRF cylinder testing programs were conducted to validate the optimal cement slurry content and cement type for CRF at AMQ, MLD and HOP. A variety of sample sizes were cast, as shown in Figure 8. The Particle size distribution (PSD) is essential for CRF in all operations. The main difference between conventional and Arctic CRF lab testing is the importance of temperature. Given limitations on strength gain from the cement slurry curing under Arctic conditions, further attention should be paid to the optimal PSD and sourcing unfrozen waste material. Accordingly, a lab testing program developed in collaboration with Lafarge included the installation of thermocouples inside the samples, curing at low temperatures to better reproduce Arctic conditions, and rigorous PSD measurements.

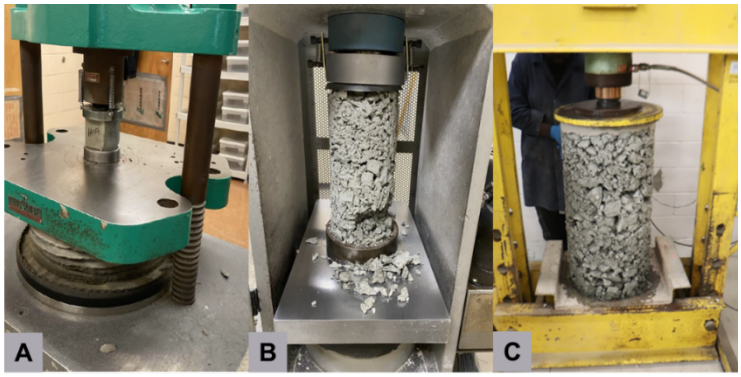

Figure 8 3 types of samples: (A) 2''x 2''mortar cube, (B) 6''x 12'' cylinder and (C) 18''x 36''cylinder.

For this paper, the results of twenty-nine 18''X 36'' cylinders, prepared with HE cement slurries (3,4 and 5% by mass) at 10°C and cured at 4°C for 7, 28 and 56 days, are discussed. The maximum particle size was limited to 1/3 of the sample diameter. Figure 9 presents the results of the 29 cylinders made with AMQ waste material. There appears to be a weak correlation between sample mass and UCS values due to the segregation of the waste material. Fundamentally, this phenomenon highlights the high variability in resistance for CRF samples, stemming primarily from the variability in PSD of the waste material. At the sample size and lab scale, segregation refers to two phenomena. Firstly, heavier samples may have less void space and a more well-graded particle size distribution, allowing for a denser waste rock packing. Segregation also refers to the preferential coating of fines and consumption of the cement slurry. In terms of results outlined in Figure 9, the samples with 5% HE cement show significant strength variability mainly due to their different PSD curves that generate variation in mass. Depending on particle arrangements, we could get higher or lower mass that controlled most of the samples' resistance no matter the recipe. The average UCS values for 3, 4 and 5% are 0.8, 1.12 and 1.44 MPa, respectively.

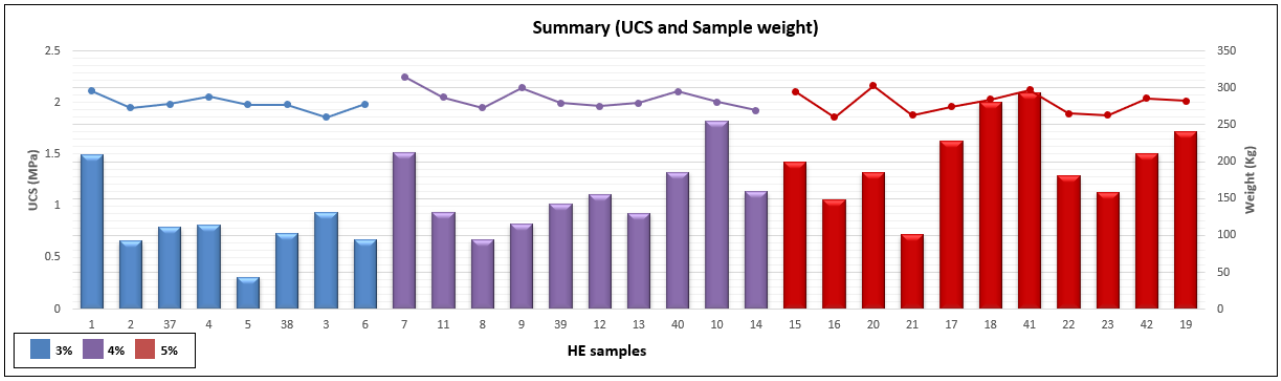

Figure 9 AMQ UCS values for CRF cylinders with 3, 4 and 5% with sample weight of each sample in kg.

During the 2020 AMQ lab campaign, another set of 8 cylinders (45.72 cm by 91.44 cm) was cured at 0°C with thermocouples to try and reproduce an extreme arctic environment. Since the samples were equipped with thermocouples, it was possible to measure the time required to reach 0°C. The results from Table 3 were obtained with material at a controlled temperature of 10°C but mixed at lab temperature. Data in Table 3 show that it took between 24 to 31 hours to reach 0°C. Although these tests do not perfectly reproduce UG conditions, they demonstrate how vital the first hours of curing are. Two different types of samples were prepared at 3, 4 and 5% cement slurry. The first set was mixed with fresh water (FW) and the second with salt water, SW (10% $CaCl_2$). Without considering mechanical strength, it was possible to measure that using SW increases the time required for the samples to reach the freezing point. Increasing the time that the CRF remains above 0°C increases the duration of the hydration reaction. In southern operations where the temperature always remains above 0°C, full hydration and complete creation of cement bonds are expected. This is not necessarily the case under Arctic conditions. Results show that for 3 and 4% cement slurry, the water type does not influence the time to reach 0°C. However, for the 5% group with salt water, it took 15% longer to reach the freezing point. Considering that most of the cementation reaction occurs within 24 hours of placement (i.e., while the CRF temperatures remain above 0°C) and that salt water was available in the Arctic environment, it was decided to use process water instead of fresh water for CRF mixing both at AMQ and HOP. In addition, the flow test results presented in Table 2 indicate that the chloride concentration in the 10°C process water does not create operational issues for the CRF slurry.

Table 3 Time before reaching 0°C for 18''X 36'' cylinders cured at 0°C

Cement %	Type of water	Time before 0°C (hours)	Combined average (hours)
5% HE/GUL	FW	26	28.9
	SW	30.9	
4% HE/GUL	FW	24.2	24.6
	SW	25	
3% HE/GUL	FW	25	25.2
	SW	25.1	

It is widely accepted that a key factor governing CRF strength is the segregation of the waste rock during placement, as shown in Figure 10. Yu & Counter (1983) evaluated the in-situ resistance of CRF while drifting through a backfilled CRF stope at Kidd Creek. After one year of curing, this drift exhibited resistance variations and uneven aggregate distributions related to the segregation of particles. The highest resistance values were in the dump cone area. The strength decreased as the aggregate in the layers got coarser, and there were fewer fine points of contact. Therefore, including smaller particles (30 mm and less) in a well-graded PSD is essential, as they create the best bond between the particles and the cement slurry.

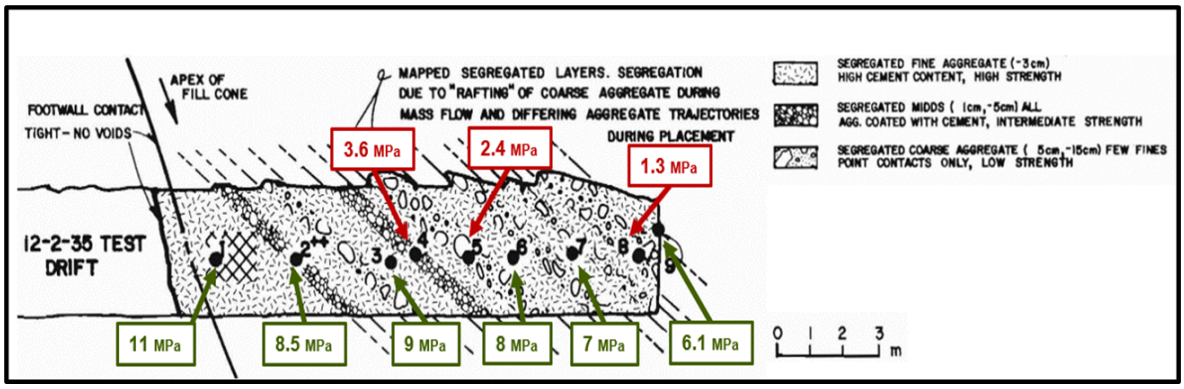

Figure 10 Schematical cross-section of a drift in CRF at Kidd Creek mine, after Yu & Counter (1983).

At most arctic operations, the surface stockpiles are frozen for much of the year. The only reliable source of unfrozen waste rock is underground development waste, but there can be significant variations in the lithologies and PSD of this material. Given the importance of PSD for CRF control quality, an attempt was made to set operational guidelines for the waste rock PSD. The lab testing program assumed conditions where the waste is unfrozen, and water and cement used to produce the slurry are at 10°C. Based on lab results from over four years of testing, it was possible to observe that the Talbot curve (Talbot & Richard 1923), as used by Swan (1985), can be helpful to validate the proper size distribution of CRF waste rock in a mining operation (Equation 1).

$$P(D) = 100 * \left(\frac{D}{D_m}\right)^n \quad (1)$$

where: n = constant (0.5 for CRF)

D = maximum aggregate particle size

D_m = % passing for each particle size

It is difficult to control the waste PSD that is available for CRF production underground. Lab testing demonstrated that the use of photogrammetry could help control CRF quality. Photogrammetry has some limitations regarding representativity, but it is more effective than traditional sieve analysis for this application (Gelinas, 2017). Each sample was photographed in the mixer and analysed using photogrammetry to produce its specific PSD curve. For 39 out of 46 AMQ samples, the theoretical Talbot curve (Equation 1) was compared to the individual PSD curves, grading from F10 to the maximum size. Then these 10 grading differences were averaged to obtain an overall average difference for each sample compared to the Talbot curve. It was possible to then calculate the difference of UCS from individual samples relative to their group average (groupings based on a percentage of cement at 3%, 4% and 5%).

Table 4 presents data from the 5% group. The average UCS is 1.54 MPa for the group of samples within 10% of the Talbot curve. The average goes down to 1.21 MPa if the grading is over 10% different from the Talbot curve. With the same cement percentage, a group of samples closer to the ideal particle size distribution from Talbot can be 34% stronger in terms of UCS. The data are not all included in the table below, but for the 4% group, the average UCS for the group of samples closer to the Talbot curve is 1.25 MPa; only 1.11 MPa for the group of samples are more than 10% away from Talbot curve. Important to note here that the average was made not taking into account the curing time since it was assumed that most of the resistance developed within the first days.

Table 4 UCS results with HE cement (SW – saline process water, FW – freshwater)

Mix #	Cement %	Type of Cement	Breaking time	Type of water	Weight (Kg)	UCS (MPa)	Diff. from Talbot (total)	UCS (MPa) group average
17	5%	HE	28 days	FW	274	1.63	7%	1.54
41	5%	HE	28 days	FW	297	2.10	7%	
22	5%	HE	28 days	SW	265	1.29	7%	
23	5%	HE	28 days	SW	263	1.13	10%	
21	5%	HE	7 days	SW	263	0.72	11%	1.21
16	5%	HE	7 days	FW	260	1.06	15%	
20	5%	HE	7 days	SW	303	1.32	16%	
15	5%	HE	7 days	FW	295	1.42	20%	
42	5%	HE	28 days	SW	286	1.51	40%	

AMQ CRF testing lab results show that a tolerance of ±10% deviation from the Talbot curve does not significantly alter the optimised UCS values. These results were used to set initial waste rock PSD guidelines for our Arctic UG operations. The operations have slowly implemented this part of their QA/QC program, using PSD generated from pictures of the waste used for CRF. Figure 11 is an example of a picture taken underground at AMQ. The photogrammetry software calculates PSD curves that can then be plotted graphically. This allows the waste used at a specific time and place to be compared to the optimal PSD defined by Talbot ±10%.

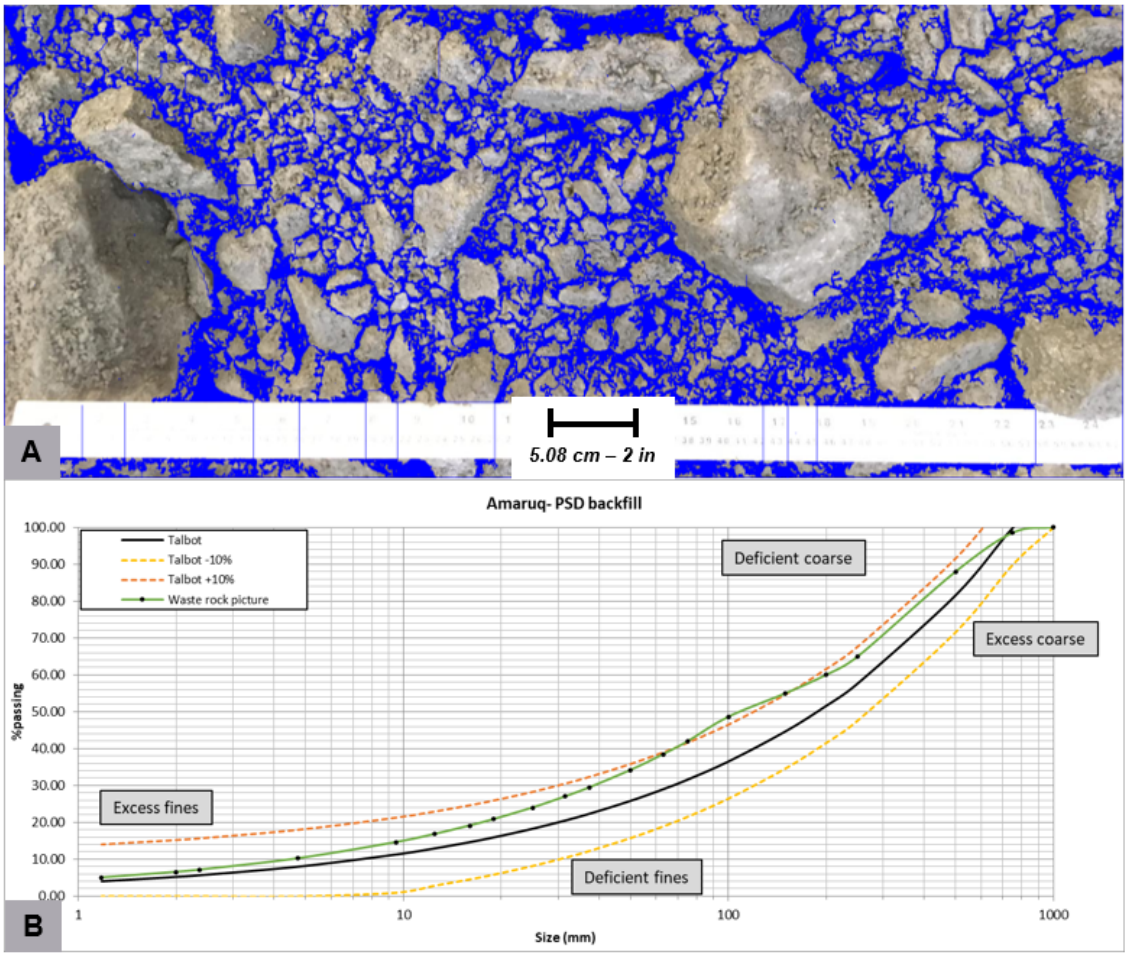

Figure 11 Particle contours automatically generated in a photogrammetry software (a), and results plotted graphically relative to the Talbot curve ±10% tolerance (b).

This photogrammetry technique is slightly less precise than a traditional sieve analysis. However, it is much faster and more effective and does not require any lab or specialised technical staff. This technique can be used by any engineering team member underground, with pictures taken directly in the LHD bucket without affecting the efficiency of the backfilling process.

7 Conclusion

This paper proposes efficient, simple tests that can be done either in a lab or UG with simple instrumentation to reduce backfill quality uncertainty. Considering temperature measurements, water chemistry or Particle Size Distribution, this paper describes the application of engineering best practices to backfill design and optimisation in AEM mines operating in the Canadian Arctic. From the application of these testing methods, in collaboration with external partners, several elements can be highlighted as key takeaways for Arctic backfill design:

- Low curing temperatures highly affect the development of mechanical strength. Therefore, HE cement is recommended as an alternative to GU cement at lower temperatures (4°C) since it is more effective at generating HE-age resistance.
- The salt content (calcium chloride and sodium chloride) of the interstitial tailings and mixing waters also influences mechanical strength development. Therefore, the mechanical strength can be impacted positively or negatively depending on the concentration and main ion types.
- Daily temperature measurements with a handheld laser thermometer should be used to validate the temperature of CRF and CPB constituents and ambient rock mass conditions. These readings can be used to set standard operating temperature values and adjust Arctic operations' QA/QC testing programs to better represent their temperature and curing conditions.
- Simple flow tests and water chemistry analyses should be done sporadically to flag issues with the mixing water chemistry and binder interaction. Once determined, a range of acceptable ion concentrations can be used as an opportunity to increase the resistance of CRF and reuse UG water instead of fresh water.
- Photogrammetric analysis can efficiently measure the waste rock PSD, which can be compared by the Talbot curves to optimise CRF strength. Laboratory testing data from two operations with different maximum particle sizes indicate that a tolerance ± 10% from the Talbot curve is acceptable to optimise CRF resistance for a given slurry recipe.

Acknowledgement

The authors would like to acknowledge all the support from operations and the numerous technical personnel involved in backfill research at the different stages of these initiatives, specifically from Meliadine (Jawad Haloui, Louis-Philippe Cyr, Nicolas St-Onge), Amaruq (Claude Gagné, Mathieu Hotte), Hope Bay (Philemon Desrochers-Gagnon and Pierre-Olivier Lamontagne), and CSD (Véronique Falmagne and François Petrucci). In addition, a special thank you goes to the technical team from the Lafarge Holcim lab and, more importantly, to Marie-Andrée Guindon. Another special acknowledgement goes to all present and past technical staff of the URSTM at UQAT Rouyn-Noranda and to David Stone from MineFill Services.

References

AEM 2022, *Operations Overview*, Agnico Eagle Mines, viewed 1 December 2022, https://www.agnicoeagle.com/English/operations/default.aspx

ASTM International 2011, *Standard Test Method for Compressive Strength of Hydraulic Cement Mortars Using 50-mmCube Specimens* (C109/C109M-11), ASTM International, West Conshohocken.

Beya, FK 2016, *Étude du Transfert de Chaleur dans les Remblais en Pâte Cimentés Curant Sous les Conditions aux Frontières des Chantiers Miniers dans le Pergélisol* (Study of Heat Transfer in Curing Cemented Paste Under Boundary Conditions of Mine Workings in Permafrost). MSc thesis, Université du Québec, Abitibi Témiscamingue.

De la Vergne, J 2000, *Hard Rock Miners Handbook*. McIntosh Engineering Limited, North Bay.

Gélinas, LP 2017, *Caractérisation des Propriétés Géomécaniques des Barricades Rocheuses et des Chantiers Miniers Remblayés en Vue de leur Analyse de Stabilité* (Characterisation of the Geomechanical Properties of Rock Barricades and Backfilled mine Workings for their Stability Analysis), MSc thesis, Polytechnique de Montréal, Montréal.

Hughes, PB 2014, *Design Guidelines: Underhand Cut and Fill Cemented Paste Backfill Sill Beams*, PhD thesis, University of British Columbia, Vancouver.

Kalonji, PK 2016 *Étude des Propriétés Rhéologiques et du Transport du Remblai Cimenté en Pâte en Conditions Nordiques* (Study of the Rheological Properties and Transport of Cemented Paste Backfill Under Northern Conditions), MSc thesis, Université du Québec, Abitibi-Témiscamingue.

Lafarge 2020, *Amaruq CRF Testing Results and Pictures*, Lafarge Technical memorandum #1, Technical lab of Montréal, Montréal, pp. 1-5.

Swan, G 1983, Compressibility Characteristics of a Cemented Backfill, *CIM Bulletin*, vol. 76, no. 856, p. 22.

SRK 2017, *Hydrogeological Characterisation and Modeling of the Proposed Boston, Madrid South and Madrid North Mines, Hope Bay Project, Package P5-13*, Environmental impact statement, vol. 1, annex V1-7, Type A Water Licence Applications, pp. 1-113.

Talbot, AN & Richard, F 1923, 'The Strength of Concrete: Its Relationship to the Cement, Aggregates and Water', *University of Illinois Bulletin*, no. 137, pp. 5-115.

URSTM 2012, *Paste Backfill Optimisation for the Meliadine Mine Project*, final report PU-2012-06-728, URSTM, Rouyn-Noranda, pp. 1-24.

URSTM 2014, *Essais Additionnels sur Remblai Pour le Projet Meliadine (Additonal testing on cemented paste backfill for the Meliadine mine project)*, final report PU-2014-03-885, URSTM, Rouyn-Noranda, pp. 1-13.

URSTM 2015, *Paste Backfill Optimisation for the Meliadine Project: Phase 4*, final report PU-2014-03-887, URSTM, Rouyn-Noranda, pp. 1-28.

Yu, TR & Counter, DB 1983, Backfill practice and technology at Kidd Creek Mines, *CIM Bulletin*, vol. 76, no. 856, pp. 56-65.